Diagnostic Accuracy of Echo Envelope Statistical Modeling Compared to B-Mode and Power Doppler Ultrasound Imaging in Patients With Clinically Diagnosed Lateral Epicondylosis of the Elbow

Nathalie J. Bureau, MD, MSc ⓘD, François Destrempes, PhD, Souad Acid, MD, Eugen Lungu, MD, MSc, Thomas Moser, MD, MSc, Johan Michaud, MD, Guy Cloutier, PhD

Abbreviations

AUROC, area under the receiver operating characteristic curve; CET, common extensor tendon; CI, confidence interval; DASH, Disabilities of the Arm, Shoulder, and Hand; HKD, homodyned K distribution; IQR, interquartile range; LE, lateral epicondylosis; MSK, musculoskeletal; PD, power Doppler; QUS, quantitative ultrasound; RCL, radial collateral ligament; ROI, region of interest; US, ultrasound

Objectives—To compare the accuracy of homodyned K quantitative ultrasound (QUS) with that of B-mode and Doppler ultrasound imaging for discriminating between lateral epicondylosis (LE) and asymptomatic elbows.

Methods—This prospective study received Institutional Review Board approval, and participants provided written informed consent. Between February 2015 and March 2017, 30 LE elbows in 27 patients and 24 asymptomatic elbows in 13 volunteers underwent B-mode, Doppler, and radiofrequency ultrasound imaging of the common extensor tendon (CET) and radial collateral ligament (RCL). Two readers classified the elbows independently on the basis of a review of B-mode and Doppler images. The global and local estimates of QUS parameters (μ_n, $1/\alpha$, and k) were computed in the CET and CET-RCL regions, respectively, and the area of each region was calculated. A random-forest classifier identified the most discriminating 3-parameter combination: CET global estimate of $1/\alpha$, CET-RCL area, and local estimate of k.

Results—The patients with LE had a mean age of 50 years (range, 31–66 years), and the volunteers had a mean age of 50 years (range, 37–57 years). The area under the receiver operating characteristic curve, sensitivity, and specificity of reader 1, reader 2, and the QUS-based model were 0.80 (95% confidence interval [CI], 0.66–0.95), 0.72 (95% CI, 0.56–0.89), and 0.88 (95% CI, 0.72–1.04); 0.79 (95% CI, 0.66–0.93), 0.65 (95% CI, 0.47–0.82), and 0.84 (95% CI, 0.67–1.01); and 0.82 (95% CI, 0.80–0.85), 0.73, and 0.79, respectively.

Conclusions—An automated, computer-based QUS technique diagnosed LE with accuracy of 0.82. This technique could provide quantitative biomarkers for the characterization of LE disease.

Key Words—elbow; sensitivity; specificity; statistical models; tendons; ultrasound

Lateral epicondylosis (LE) of the elbow is a common, debilitating tendon disorder found among working-age individuals, with a substantial socioeconomic burden and no standardized care management.[1] Lateral epicondylosis is an

overuse syndrome leading to degenerative changes of the common extensor tendon (CET),[2] diagnosed clinically by the history and physical examination. Imaging is usually reserved for unclear or refractory cases or to plan surgery.[3] Ultrasound (US) is well suited for the investigation of LE because of its relative affordability and good spatial resolution.[4]

Studies examining the diagnostic and prognostic values of US in the management of LE show variable results.[5–8] In a meta-analysis, Latham and Smith[9] reported a pooled sensitivity of 0.82 (95% confidence interval [CI], 0.76–0.87) and a pooled specificity of 0.66 (95% CI, 0.60–0.72) when using US in the diagnosis of suspected LE. In another study, the presence of large intrasubstance tears and a tear of the radial collateral ligament (RCL) were associated with poorer clinical outcomes.[10] Inter-reader variability,[6,11] limited specificity,[9] and the qualitative assessment provided by US currently restrict its value as a diagnostic method.

New technologies, known as quantitative ultrasound (QUS) imaging techniques, are emerging and appear promising in the characterization of the biomechanical, acoustical, and structural properties of tissues.[12] Among these techniques, several methods aim at characterizing tissue microstructures based on statistical modeling of the echo envelope, ie, the unfiltered, uncompressed reconstructed B-mode image, with statistical parameters that have a physical interpretation.[13] A study has recently demonstrated the potential of homodyned K distribution (HKD) modeling of the echo envelope in a series of 96 consecutive indeterminate solid breast lesions, in which 26% of biopsies could have been avoided on the basis of the statistical model classification.[14] Hence, by providing numeric values associated with tissue characteristics, QUS can increase the specificity of imaging findings, potentially helping clinicians define classification schemes of diseases more accurately and stratify care management options.

We hypothesized that HKD QUS tissue characterization would be able to assess the process of tendon degeneration associated with LE. As a first step toward this goal, this study aimed to compare the accuracy of HKD echo envelope statistical modeling with that of B-mode US combined with power Doppler (PD) imaging for discriminating between clinically diagnosed LE and asymptomatic elbows.

Materials and Methods

This prospective study was approved by the Centre Hospitalier de l'Université de Montréal Institutional Review Board (CE 14.167), and participants provided written informed consent.

Participants

Patients with a clinical diagnosis of LE established by a physiatrist, a sports medicine physician, an orthopedist, or an occupational medicine specialist referred to our musculoskeletal (MSK) US clinic were asked to participate in the study. Patients were excluded if they had a history of lateral elbow corticosteroid injection within the past 3 months, elbow fracture or surgery, percutaneous treatment of LE, or arthritis. A research assistant evaluated the participant's level of lateral elbow pain on resisted wrist extension, using a numeric pain scale ranging from 0 (no pain) to 10 (worse pain imaginable), and measured the participants' pain-free maximum grip strength[15] using a Jamar Plus+ dynamometer (Jamar, Park City, UT). The participants completed the shortened versions of the Disabilities of the Arm, Shoulder, and Hand (QuickDASH) disability/symptoms and work modules.[16] An age-matched group of asymptomatic volunteers who declared no history of LE and who did not meet the exclusion criteria were recruited from the hospital community and examined in the same fashion. A participant flowchart is presented in Figure 1.

B-Mode US and PD Imaging

A B-mode US and PD imaging examination was performed either by a fellowship-trained MSK radiologist with 23 years of experience in MSK US or a second-year fellow in MSK radiology using an Acuson S3000 US scanner (Siemens Healthineers, Mountain View, CA) with a standardized imaging protocol and either a linear 14L5SP- or 14 L5-MHz transducer. The participants were seated, with the pronated forearm resting on an examination table and the elbow flexed at 70°.[6,17] Long- and short-axis dynamic scans were acquired from anterior to posterior and from proximal to distal, respectively, spanning the entire CET and RCL. A PD imaging evaluation was performed in the long axis,[18] and a static image showing the maximum Doppler signal was recorded.

B-Mode US and PD Imaging Analysis

One fellowship-trained MSK radiologist and 1 fellowship-trained physiatrist, with 10 and 11 years of experience in MSK US, respectively, were familiarized with the grading scheme (Table 1) based on previously described US anatomy of the CET and RCL[19] and US findings of LE.[20] Both readers, blinded to the clinical status of the participants, reviewed the US cine clips (Videos 1 and 2) and the PD image (Figure 2) independently, using diagnostic software (Syngo.via, VB10B; Siemens AG, Munich, Germany) on a picture archiving and communication system workstation.

Quantitative US Data Acquisition

The MSK radiologist with 23 years of experience obtained a long-axis, 3-second radiofrequency US image sequence of the CET and RCL using a Terason t3000 US scanner (Teratech, Burlington, MA) equipped with a linear 12 L5-MHz transducer.[14] The image sequence was acquired on the image, showing a small groove at the base of the lateral epicondyle to ensure consistency in data acquisition between participants (Figure 3).

Quantitative US Data Analysis

The radiofrequency US images were transferred to a workstation and given a numeric identifier. The contours of a region of interest (ROI) encompassing both the CET and the RCL (CET-RCL ROI) were manually delineated by the MSK radiologist with 23 years of experience, who was blinded to the clinical status of the participants, on the first frame of the radiofrequency sequence. Delineation of the ROI was then propagated automatically in subsequent frames of the sequence by a segmentation algorithm.[21] Contours of the region composed solely of the CET[19] (CET ROI) were computed automatically from the CET-RCL ROI by joining the lower and upper borders of the latter region with the perpendicular bisector of its lower border (Figure 3).

The echo envelope was reconstructed from US radiofrequency signals in MATLAB software (The MathWorks, Natick, MA)[22] and then modeled by a single HKD within the CET ROI,[23] thus yielding a single global estimate, ie, estimated on all pixels within the ROI. Three statistical parameters describing the HKD were estimated according to a previously described method:[24] (1) μ_n, the mean intensity normalized by its maximum value; (2) the reciprocal $1/\alpha$ of the scatterer clustering parameter α; and (3) k, the coherent-to-diffuse signal ratio. The parameter μ_n is kindred to the normalized echogenicity in B-mode images. Parameter $1/\alpha$ is an indicator of

Figure 1. Participant flowchart.
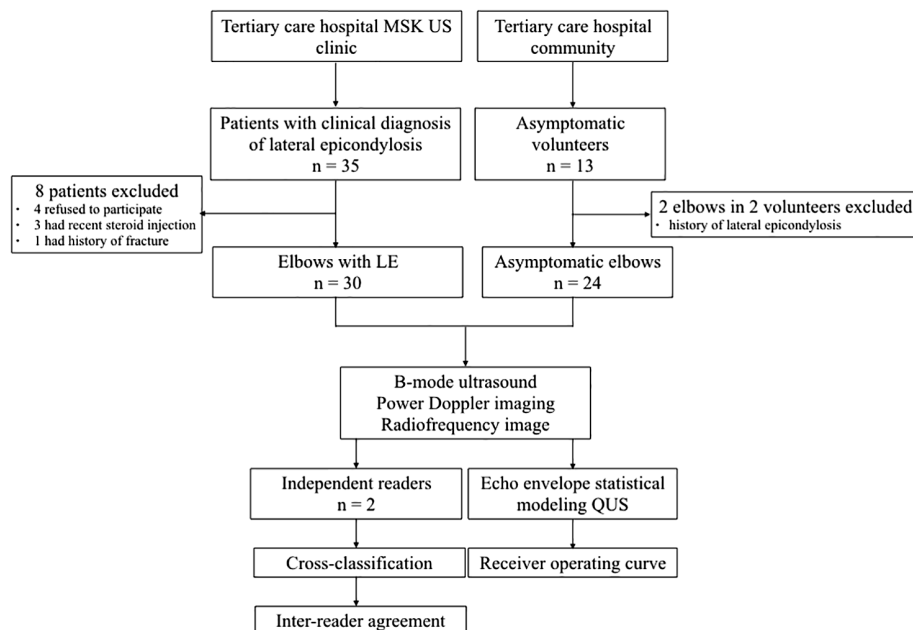
inhomogeneity in acoustical fluctuations within the scattering tissue.[25] Parameter k measures the amount of the structure, as opposed to randomness, within the spatial organization of scatterers.[23,24] To characterize the tissue on a finer scale and to allow for tissue variability between the CET and the RCL, the 3 HKD parameters were also estimated locally, ie, estimated in local windows to produce parametric maps, as previously described.[26] For each HKD parametric image, the mean and interquartile range (IQR) values were calculated. Finally, the CET and CET-RCL ROI areas were measured.

Therefore, a total of 11 features, including global estimates of μ_n, $1/\alpha$, and k parameters within the CET ROI, mean and IQR of μ_n, $1/\alpha$, and k parametric maps

within the CET-RCL ROI, and the areas of the CET and CET-RCL ROIs, were computed. Implementation in Visual C++ (Microsoft Corporation, Redmond, WA) and MATLAB programming languages and all analyses were performed by a mathematician with 27 years of experience, who was blinded to the clinical status of the participants.

Statistical Analyses

A generalized estimating equation model based on a binomial distribution with an identity link function and an exchangeable correlation matrix was used to calculate estimates of sensitivity and specificity for B-mode US and PD categorical variables. The area under the receiver operating characteristics curve (AUROC) was computed for the maximum CET thickness.[27] Inter-reader agreement was assessed by Cohen κ for dichotomous US parameters. Ultrasound and PD imaging parameters with multiple categories were assessed as multiple-category data and as dichotomized data in 0 versus 1 or higher and compared with the clinical diagnosis as the reference standard. For the mean maximal thickness of the CET, inter-reader agreement was assessed with the intraclass correlation coefficient based on a linear mixed model. All analyses accounted for the patient cluster effect due to the presence of observations for both elbows within the same patients. The 2 readers were considered as belonging to a random sample to generalize the results to other readers.[28] Statistical analyses were performed by a biostatistician using SAS software

Table 1. B-Mode US and PD Imaging of the CET and RCL Grading Schemes

| Imaging Features	Measurement or Grading Score
Maximal tendon thickness[a]	cm
Tendon echogenicity	Grade 0: normal hyperechoic fibrillar appearance
	Grade 1: hypoechogenicity over small tendon surface area
	Grade 2: hypoechogenicity over moderately large tendon surface area
	Grade 3: hypoechogenicity of tendon with anechoic fissures
	Grade 4: full-thickness tendon tear or tendon disinsertion
Enthesophyte	Grade 0: absent
	Grade 1: present
Calcifications	Grade 0: absent
	Grade 1: hyperechoic without acoustic shadowing
	Grade 2: hyperechoic with acoustic shadowing
RCL echo structure	Grade 0: normal hyperechoic fibrillar appearance
	Grade 1: hypoechoic, thickened or torn
PD US	Grade 0: no pixel
	Grade 1: a few pixels
	Grade 2: ≤50% of tendon surface
	Grade 3: ≥50% of tendon surface
Cortical irregularities	Grade 0: absent
	Grade 1: present
Diagnostic impression	Grade 0: asymptomatic volunteer
	Grade 1: patient with LE

[a]Maximal tendon thickness was measured on a long-axis scan at the base of lateral humeral epicondyle.

Figure 2. Image from a 49-year-old female patient presenting with LE of the right elbow of 2 months' duration. Long-axis PD US shows grade 2 (≤50% of the tendon surface involved) neovascularity within a hypoechoic thickened CET and RCL complex. H indicates lateral humeral epicondyle; and R, radial head.
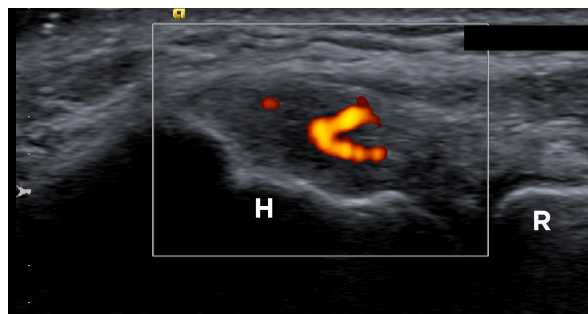
(version 9.4; SAS Institute Inc, Cary, NC). $P < .05$ was considered to indicate a significant difference.

Regarding QUS data, statistical learning based on a random-forest classifier[29] was performed on the database using the 11 features. Feature selection was performed with random forests of 3000 decision trees each, on all combinations of at most 3 features to avoid overfitting, by retaining the 10 combinations with the highest geometric mean for sensitivity and specificity.[30] A maximum of 3 features was adopted to avoid overfitting due to model complexity versus the sample size. For each of the 10 selected combinations of features, the curve was built by generating stratified samples with sample proportion in one class varying from 1/40 to 39/40 by steps of 1/40. For each specified proportion, the training and cross-validation errors were combined according to the 0.632+ bootstrap method[31] using 1000 bootstraps on participants. In cases in which both elbows of a participant were examined, a weight of ½ was assigned to each elbow in the computation of true- and false-positive rates. To further address overfitting due to model complexity, trees were restricted to a maximum of terminal nodes ranging from 2 to 20 by steps of 2. Areas under the receiver operating characteristic curve were then computed by the trapezoid method, one for each maximal number of terminal nodes, and the combination of features with the highest AUROC was selected as the best-found combination. For the best combination, the 95% CI was estimated from percentiles of a sample of AUROCs generated from the jackknife method[32] as a leave-one-subject-out cross-validation.

Figure 3. Reconstructed radiofrequency images of the right CET and RCL in a 49-year-old female patient with LE. **A**, The US transducer was positioned in the long axis over the lateral humeral epicondyle (H) during a 3-second radiofrequency cine sequence acquisition. A small groove (arrow) at the base of the lateral epicondyle was used as a landmark to ensure consistency in data acquisition between participants. **B**, An MSK radiologist manually delineated the contours of the CET and RCL (CET-RCL ROI), as shown by the white lines, on the first image frame. Thereafter, this ROI was propagated automatically on the subsequent frames of the cine sequence by a segmentation algorithm. **C**, From the CET-RCL ROI, the region of the CET, referred to as the CET ROI, was automatically segmented by an algorithm that joined the upper and lower borders of the CET and RCL with the perpendicular bisector of the lower border, as it was shown in a cadaveric study that the CET occupies approximately 50% of the humeral footprint, whereas the remaining distal footprint is the site of the RCL attachment. R indicates radial head.
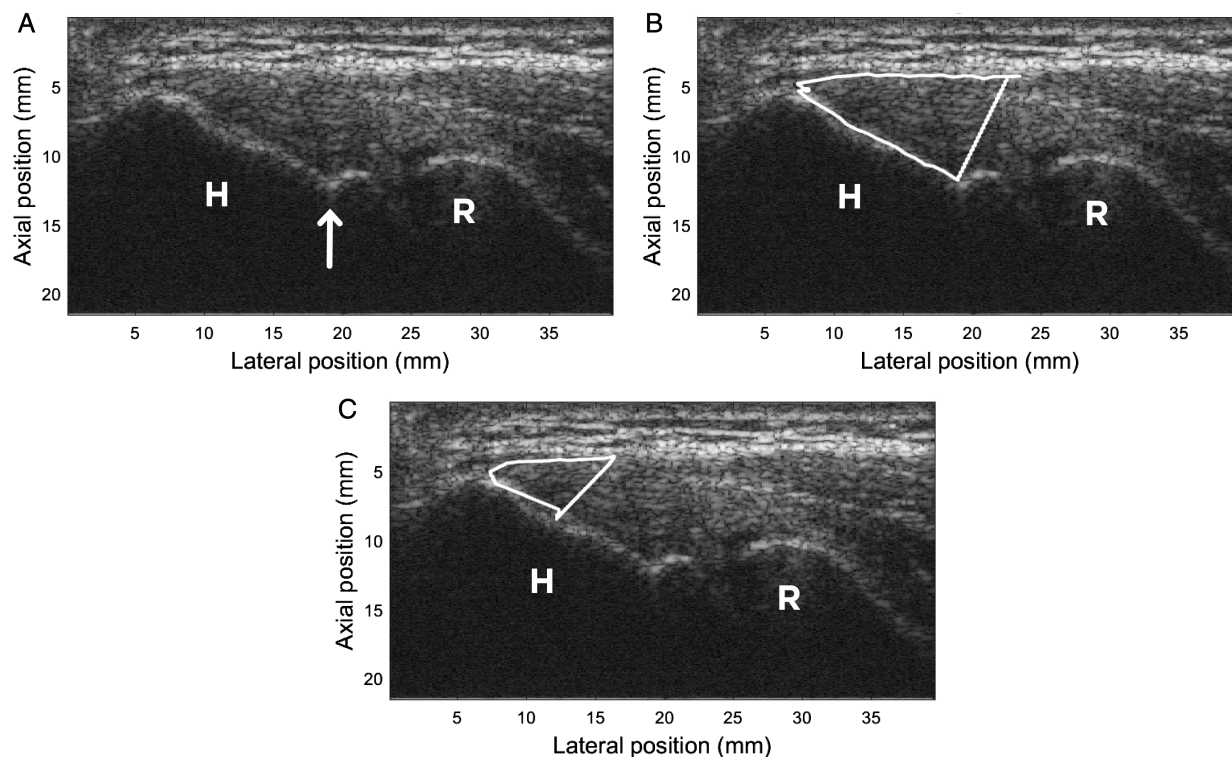
The statistical analysis was performed with the statistical software R (version 3.2.5, 2016; R Foundation for Statistical Computing, Vienna, Austria) by the same mathematician, who was unblinded for this task.

Results

Participants
Between February 2015 and March 2017, 30 LE elbows in 27 patients, including 12 men (mean age, 50.8 years; range, 31–66 years) and 15 women (mean age, 49.8 years; range, 40–57 years), presenting with a mean duration of symptoms ± SD of 29 ± 27 months (range, 2–120 months) were imaged (Table 2). Three patients had both elbows diagnosed with LE. The asymptomatic cohort consisted of 13 volunteers, including 6 men (mean age, 52.1 years; range, 45–57 years) and 7 women (mean age, 47.7 years; range, 37–56 years). Eleven volunteers had both elbows examined, and 2 other volunteers had a single elbow examined, for a total of 24 asymptomatic elbows. The groups were comparable in terms of mean age ($P = .79$), sex distribution ($P > .99$), and side examined ($P = .78$). The patients with LE had higher pain scores ($P < .0001$) and functional impairment scores (QuickDASH general and work modules, $P < .0001$) and lower grip strength ($P = .0001$) than the volunteers.

B-Mode US and PD Imaging
Table 3 presents the results of the B-mode and PD imaging parameter analysis by the readers. For the US parameter maximum tendon thickness, the AUROCs were 0.80 (95% CI, 0.66–0.95) and 0.79 (95% CI, 0.66–0.93), respectively, for readers 1 and 2, with almost perfect inter-reader agreement (intraclass correlation coefficient, 0.84).[33] As determined by the closest top-left method on the receiver operating characteristic curve, thresholds of 0.54 and 0.59 cm for readers 1 and 2 yielded a sensitivity of 0.80 and a specificity of 0.79 for reader 1 and a sensitivity of 0.73 and a specificity of 0.83 for reader 2.

Table 4 presents the sensitivity, specificity, and inter-rater agreement for the categorical B-mode US and PD parameters for both readers. Regarding the diagnostic accuracy at identifying LE elbows, reader 1 had a sensitivity of 0.72 (95% CI, 0.56–0.89) and a specificity of 0.88 (95% CI, 0.72–1.04), and reader 2 had a sensitivity of 0.65 (95% CI, 0.47–0.82) and a specificity of 0.84 (95% CI, 0.67–1.01), with almost perfect inter-reader agreement ($\kappa = 0.81$). For both readers, tendon echogenicity was the most sensitive (reader 1, 0.93 [95% CI, 0.83–1.02]; reader 2, 0.89 [95% CI, 0.78–1.00]) but least specific (reader 1, 0.35 [95% CI, 0.10–0.60]; reader 2, 0.25 [95% CI, 0.07–0.43]) US parameter, with moderate inter-rater agreement ($\kappa = 0.47$) on the dichotomized grading score. Inter-rater agreement was highest ($\kappa = 1.00$) for the dichotomized PD imaging grading score.

Quantitative US Data
The best combination of at most 3 parameters consisted of the following features: area of the CET-RCL ROI, global estimate of the $1/\alpha$ parameter in the

Table 2. Comparison of Demographic and Clinical Characteristics Between Patients With LE and Asymptomatic Volunteers

Variable	Patients	Volunteers	P^a
Participants, n	27	13	
Men, n (%)	12 (44.4)	6 (46.2)	>.99
Women, n (%)	15 (55.6)	7 (53.8)	
Age, y	50.2 ± 7.6	49.7 ± 6.3	.79
	(31–66)	(37–57)	
Elbows, n	30	24	
Side, n (% of tendons)			.78
Right	16 (53.3)	11 (45.8)	
Left	14 (46.7)	13 (54.2)	
Symptom duration, mo	29.4 ± 26.8	0.0	
	(2.0–120.0)		
Treatment received, n (% of tendons)	21 (70.1)	0 (100.0)	
Surgery	0 (100.0)	0 (100.0)	
Percutaneous treatment	0 (100.0)	0 (100.0)	
Physical therapy	15 (50.0)	0 (100.0)	
Steroid injections	16 (53.3)	0 (100.0)	
Other	10 (33.3)	0 (100.0)	
Pain on resisted wrist extension	5.2 ± 2.0	0.0	<.0001
	(1.0–9.0)		
Grip strength elbow extended, kg	17.6 ± 13.1	34.4 ± 13.4	.0001
	(2.0–54.0)	(18.0–59.0)	
QuickDASH general module	47.4 ± 17.7	0.6 ± 1.4	<.0001
	(13.6–70.5)	(0.0–4.6)	
QuickDASH work module	50.9 ± 29.2	0.0	<.0001
	(0.0–100.0)		

Data are presented as mean ± SD (range) where applicable. For QuickDASH general and work modules, each module score is calculated out of 100, with a higher score indicating a worse status.
[a]Student *t* or Fisher exact test.

CET ROI (Figure 4), and IQR of the k parametric map in the CET-RCL ROI (Figure 5). For this combination of features, the AUROC was 0.82 (95% CI, 0.80–0.85). The sensitivity was 0.73 and the specificity was 0.79, as determined by the closest top-left method on the receiver operating characteristic curve.

Discussion

One million individuals have a diagnosis of LE each year in the United States.[1] The clinical course of LE is unpredictable, and a typical episode will last, on average, between 6 months and 2 years.[1] Currently, the role of imaging in guiding care management is limited. In this study, 2 readers obtained moderate sensitivity (0.72 and 0.65) and high specificity (0.88 and 0.84) with almost perfect inter-reader agreement ($\kappa = 0.81$) in discriminating LE and asymptomatic elbows. The readers based their diagnostic impression on the review of B-mode US cine clips and a single PD static image of the CET and RCL, thus integrating and weighting all imaging findings to arrive at a diagnosis. Our results showed slightly lower sensitivity (0.77–0.97) and higher specificity (0.47–0.73) than prior studies.[8,9,18,34] When US imaging parameters were considered individually, our results generally showed moderate-to-high sensitivity but moderate-to-low specificity, as asymptomatic elbows in middle-aged individuals commonly present with positive US findings of LE.[8,34]

In current practice, the only quantitative US parameter used to characterize LE is CET thickness. In this present study, CET thickness, as assessed by

Table 3. Results of B-Mode US and PD Imaging Parameter Analysis by 2 Independent Readers

	Reader 1		Reader 2	
Imaging Parameter	Patients	Volunteers	Patients	Volunteers
Maximal tendon thickness, cm	0.60 ± 0.09 (0.43–0.83)	0.51 ± 0.07 (0.44–0.68)	0.63 ± 0.10 (0.48–1.00)	0.54 ± 0.06 (0.45–0.70)
Tendon echogenicity, n				
Grade 0	3	9	3	6
Grade 1	7	11	14	9
Grade 2	11	1	7	6
Grade 3	9	3	5	3
Grade 4	0	0	1	0
Enthesophyte, n				
Grade 0	12	15	14	16
Grade 1	18	9	16	8
Calcifications, n				
Grade 0	20	18	22	18
Grade 1	8	6	7	6
Grade 2	2	0	1	0
RCL echo structure, n				
Grade 0	5	5	23[a]	20
Grade 1	25	19	6	4
PD US, n				
Grade 0	7	16	7	16
Grade 1	3	5	5	4
Grade 2	14	3	13	4
Grade 3	6	0	5	0
Cortical irregularities, n				
Grade 0	14	18	22	20
Grade 1	16	6	8	4
Diagnostic impression, n				
Grade 0	9	21	11	20
Grade 1	21	3	19	4

Data are presented as mean ± SD (range) where applicable.
[a]Reader 2 considered that the RCL echo structure could not be evaluated in 1 case.

each reader, yielded AUROCs of 0.80 (95% CI, 0.66–0.95) and 0.79 (95% CI, 0.66–0.93), with almost perfect inter-reader agreement (intraclass correlation coefficient, 0.84). Threshold values of 0.55 cm for reader 1 and 0.59 cm for reader 2 yielded good sensitivity and specificity for reader 1 (0.80 and 0.79) and reader 2 (0.73 and 0.83). Lee et al[5] previously reported a sensitivity of 0.78 and a specificity of 0.95 for a smaller threshold value of 0.42 cm. One of the challenges with this

measurement appears to be proper threshold selection to differentiate populations.

In this study, HKD QUS combined with a random-forest classifier yielded an AUROC of 0.82 (95% CI, 0.80–0.85), a sensitivity of 0.73, and a specificity of 0.79 in the identification of LE elbows. Although the statistical model only performed as well as B-mode and PD US evaluations, these preliminary results are promising and suggest that an automated, computer-based technique simply requiring a long-

Table 4. Sensitivity, Specificity and Inter-Rater Agreement for Categorical B-Mode US and PD Imaging Parameters

| Imaging Parameter | Reader 1 | | Reader 2 | | Cohen κ | Cohen κ |
	Sensitivity (95% CI)	Specificity (95% CI)	Sensitivity (95% CI)	Specificity (95% CI)	Dichotomous Grading Score[a]	Multiple Grading Score[b]
Tendon echogenicity	0.93 (0.83–1.02)	0.35 (0.10–0.60)	0.89 (0.78–1.00)	0.25 (0.07–0.43)	0.47	0.24
Enthesophyte	0.63 (0.45–0.81)	0.62 (0.35–0.88)	0.54 (0.35–0.72)	0.66 (0.44–0.88)	0.44	
Calcifications	0.33 (0.17–0.49)	0.76 (0.56–0.97)	0.30 (0.13–0.47)	0.76 (0.56–0.97)	0.54	0.55
RCL echo structure	0.85 (0.72–0.99)	0.21 (0.07–0.35)	0.20 (0.06–0.35)	0.85 (0.65–1.04)	0.10	
PD US	0.80 (0.65–0.94)	0.66 (0.41–0.90)	0.80 (0.65–0.94)	0.66 (0.41–0.90)	1.00	0.84
Cortical irregularities	0.54 (0.35–0.72)	0.75 (0.55–0.94)	0.26 (0.11–0.42)	0.84 (0.67–1.01)	0.50	
Diagnostic impression	0.72 (0.56–0.89)	0.88 (0.72–1.04)	0.65 (0.47–0.82)	0.84 (0.67–1.01)	0.81	

[a,b]B-mode US and PD imaging parameters with multiple categories were assessed as dichotomized data in 0 versus 1 or higher ([a]) and as multiple-category data ([b]) and compared with the clinical diagnosis as the reference standard.

Figure 4. Global estimate of the 1/α parameter computed in the CET ROI in the same 49-year-old female patient as in Figure 3 (**A**) and in a 50-year-old female asymptomatic volunteer (**B**). The color represents the global estimate of the HKD parameter 1/α in the CET ROI. This statistical parameter may be viewed as an indicator of a lack of homogeneity in acoustical fluctuations within the insonified biological tissues. The estimated values of parameter 1/α were 2.6 in the patient with LE (**A**) and 0.54 in the asymptomatic volunteer (**B**), indicating greater inhomogeneity in acoustical fluctuations associated with the degenerative process of LE. H indicates humeral epicondyle; and R, radial head.
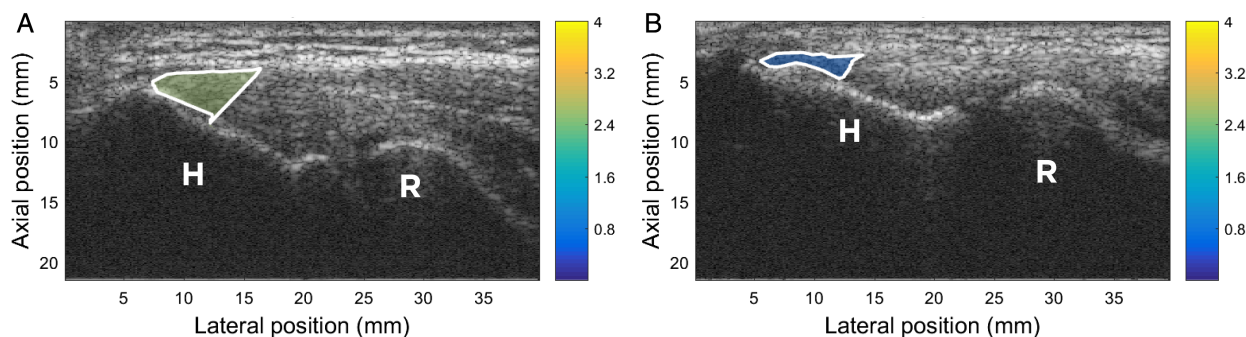
axis 3-second radiofrequency US image sequence could provide quantitative biomarkers for establishing the diagnosis of LE, as opposed to the current subjective and user-dependent qualitative imaging method.

Tendinosis leads to tendon thickening.[2] The area of the CET-RCL ROI, retained in the statistical model, reflects these changes. Moreover, tendinosis creates disparities in cell density between different regions of the tendon, with an abundance of transformed tenocytes in some degenerated areas and a disproportionate lack of cells in other areas.[2] The parameter $1/\alpha$ estimated in the CET ROI may reflect these changes, as it is regarded as a surrogate for inhomogeneity in acoustical backscatter fluctuations.[25] Tendinosis also leads to the disorganization and distortion of the collagen fibers. The IQR of the k parametric map in the CET-RCL ROI, which is indicative of the amount of structure within the spatial organization of the tissue,[23,24] may be evidenced by these histopathologic changes. Therefore, it seems reasonable to think that those quantitative biomarkers could be used in place of the conventional subjective B-mode or PD findings to provide objectively measured indicators of the disease process of LE.

Our study had several limitations. First, we used a reference standard based on a clinical diagnosis of LE. However, this was in accordance with clinical practice. Furthermore, to address this limitation, we restricted the number of included patients in whom LE was diagnosed by a specialist. Finally, our cohort of patients had definite manifestations of the disease, as indicated by the results of the numeric pain scale score, functional questionnaires, and pain-free maximum grip strength, which were all significantly different from those of the control group. Second, we did not obtain a histopathologic correlation to confirm the physical interpretation of the HKD statistical parameters. Nevertheless, considering, on the one hand, histopathologic descriptions of the degenerative process of tendinosis[2] and, on the other hand, the physical interpretation of HKD parameters,[23–25] a correlation between the two descriptors appears plausible; further studies are needed to confirm this. Third, acquisition and segmentation of the QUS data were performed by a single operator, limiting the generalizability of our results. Future studies should address the repeatability and interobserver reliability of this QUS method, as these factors are critical for the clinical translation of this promising quantitative technique.

In conclusion, an HKD technique, based on echo envelope statistical modeling and a random-forest artificial intelligence classifier, performed as well as B-mode and PD US to discriminate between clinically diagnosed LE and asymptomatic elbows, yielding an AUROC of 0.82 (95% CI, 0.80–0.85). This automated, computer-based technique could provide objectively measured imaging biomarkers for the characterization of the disease process associated with LE.

Figure 5. Parametric maps of the HKD parameter k in the CET-RCL ROI in the same 49-year-old female patient with LE (**A**) and in the same 50-year-old female asymptomatic volunteer (**B**) as in Figure 4. These parametric maps represent the local estimates of the HKD parameter k throughout the CET-RCL ROI. This parameter, called the coherent-to-diffuse signal ratio, is an indicator of the amount of structure in the spatial organization of scatterers within the insonified biological tissues. The IQR value of k was retained in the model. In the patient with LE (**A**), the IQR of k was 1.8, and that of the asymptomatic volunteer was 2.8, indicating more structural disorganization and distortion associated with the degenerative process of LE. H indicates humeral epicondyle; and R, radial head.
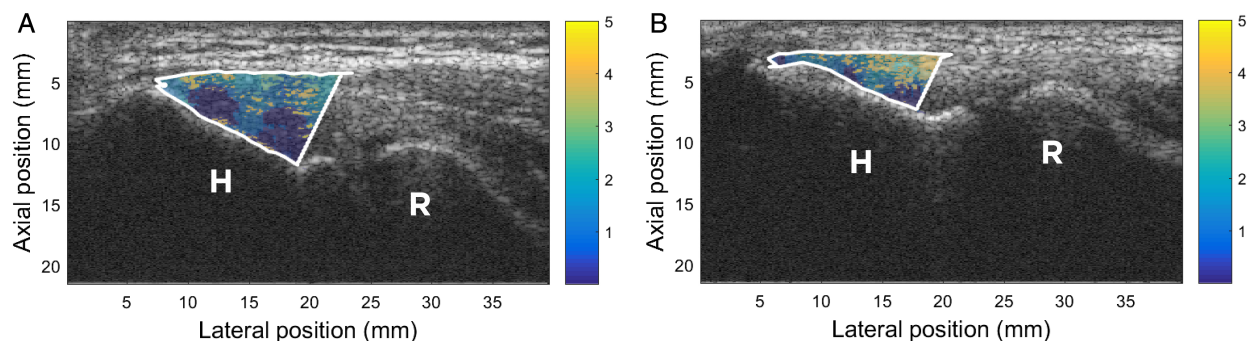
References

1. Sanders TL Jr, Maradit Kremers H, Bryan AJ, Ransom JE, Smith J, Morrey BF. The epidemiology and health care burden of tennis elbow: a population-based study. *Am J Sports Med* 2015; 43:1066–1071.

2. Järvinen M, Józsa L, Kannus P, Järvinen TL, Kvist M, Leadbetter W. Histopathological findings in chronic tendon disorders. *Scand J Med Sci Sports* 1997; 7:86–95.

3. Walz DM, Newman JS, Konin GP, Ross G. Epicondylitis: pathogenesis, imaging, and treatment. *Radiographics* 2010; 30:167–184.

4. Lee KS, Rosas HG, Craig JG. Musculoskeletal ultrasound: elbow imaging and procedures. *Semin Musculoskelet Radiol* 2010; 14:449–460.

5. Lee MH, Cha JG, Jin W, et al. Utility of sonographic measurement of the common tensor tendon in patients with lateral epicondylitis. *AJR Am J Roentgenol* 2011; 196:1363–1367.

6. Levin D, Nazarian LN, Miller TT, et al. Lateral epicondylitis of the elbow: US findings. *Radiology* 2005; 237:230–234.

7. Struijs PA, Spruyt M, Assendelft WJ, van Dijk CN. The predictive value of diagnostic sonography for the effectiveness of conservative treatment of tennis elbow. *AJR Am J Roentgenol* 2005; 185:1113–1118.

8. Heales LJ, Broadhurst N, Mellor R, Hodges PW, Vicenzino B. Diagnostic ultrasound imaging for lateral epicondylalgia: a case-control study. *Med Sci Sports Exerc* 2014; 46:2070–2076.

9. Latham SK, Smith TO. The diagnostic test accuracy of ultrasound for the detection of lateral epicondylitis: a systematic review and meta-analysis. *Orthop Traumatol Surg Res* 2014; 100:281–286.

10. Clarke AW, Ahmad M, Curtis M, Connell DA. Lateral elbow tendinopathy: correlation of ultrasound findings with pain and functional disability. *Am J Sports Med* 2010; 38:1209–1214.

11. Poltawski L, Ali S, Jayaram V, Watson T. Reliability of sonographic assessment of tendinopathy in tennis elbow. *Skeletal Radiol* 2012; 41:83–89.

12. Oelze ML, Mamou J. Review of quantitative ultrasound: envelope statistics and backscatter coefficient imaging and contributions to diagnostic ultrasound. *IEEE Trans Ultrason Ferroelectr Freq Control* 2016; 63:336–351.

13. Destrempes F, Cloutier G. Review of envelope statistics models for quantitative ultrasound imaging and tissue characterization. In: Mamou J, Oelze ML (eds). *Quantitative Ultrasound in Soft Tissues*. Dordrecht, the Netherlands: Springer; 2013:1–55.

14. Trop I, Destrempes F, El Khoury M, et al. The added value of statistical modeling of backscatter properties in the management of breast lesions at US. *Radiology* 2015; 275:666–674.

15. Smidt N, van der Windt DA, Assendelft WJ, et al. Interobserver reproducibility of the assessment of severity of complaints, grip strength, and pressure pain threshold in patients with lateral epicondylitis. *Arch Phys Med Rehabil* 2002; 83:1145–1150.

16. Franchignoni F, Vercelli S, Giordano A, Sartorio F, Bravini E, Ferriero G. Minimal clinically important difference of the Disabilities of the Arm, Shoulder and Hand outcome measure (DASH) and its shortened version (QuickDASH). *J Orthop Sports Phys Ther* 2014; 44:30–39.

17. Konin GP, Nazarian LN, Walz DM. US of the elbow: indications, technique, normal anatomy, and pathologic conditions. *Radiographics* 2013; 33:E125–E147.

18. du Toit C, Stieler M, Saunders R, Bisset L, Vicenzino B. Diagnostic accuracy of power Doppler ultrasound in patients with chronic tennis elbow. *Br J Sports Med* 2008; 42:872–876.

19. Jacobson JA, Chiavaras MM, Lawton JM, Downie B, Yablon CM, Lawton J. Radial collateral ligament of the elbow: sonographic characterization with cadaveric dissection correlation and magnetic resonance arthrography. *J Ultrasound Med* 2014; 33:1041–1048.

20. Chiavaras MM, Jacobson JA, Carlos R, et al. IMpact of Platelet Rich plasma OVer alternative therapies in patients with lateral Epicondylitis (IMPROVE): protocol for a multicenter randomized controlled study—a multicenter, randomized trial comparing autologous platelet-rich plasma, autologous whole blood, dry needle tendon fenestration, and physical therapy exercises alone on pain and quality of life in patients with lateral epicondylitis. *Acad Radiol* 2014; 21:1144–1155.

21. Destrempes F, Meunier J, Giroux MF, Soulez G, Cloutier G. Segmentation of plaques in sequences of ultrasonic B-mode images of carotid arteries based on motion estimation and a Bayesian model. *IEEE Trans Biomed Eng* 2011; 58:2202–2211.

22. Kallel F, Bertrand M, Meunier J. Speckle motion artifact under tissue rotation. *IEEE Trans Ultrason Ferroelectr Freq Control* 1994; 41:105–122.

23. Dutt V, Greenleaf JF. Ultrasound echo envelope analysis using a homodyned K distribution signal model. *Ultrason Imaging* 1994; 16:265–287.

24. Destrempes F, Poree J, Cloutier G. Estimation method of the homodyned K-distribution based on the mean intensity and two log-moments. *SIAM J Imaging Sci* 2013; 6:1499–1530.

25. Weng L, Reid JM, Shankar PM, Soetanto K. Ultrasound speckle analysis based on the K distribution. *J Acoust Soc Am* 1991; 89:2992–2995.

26. Destrempes F, Franceschini E, Yu FT, Cloutier G. Unifying concepts of statistical and spectral quantitative ultrasound techniques. *IEEE Trans Med Imaging* 2016; 35:488–500.

27. Obuchowski NA. Nonparametric analysis of clustered ROC curve data. *Biometrics* 1997; 53:567–578.

28. Shrout PE, Fleiss JL. Intraclass correlations: uses in assessing rater reliability. *Psychol Bull* 1979; 86:420–428.

29. Breiman L. Random forests. *Machine Learn* 2001; 45:5–32.

30. He H, Garcia EA. Learning from imbalanced data. *IEEE Trans Knowledge Data Eng* 2009; 21:1263–1284.

31. Efron B, Tibshirani R. Improvements on cross-validation: the .632 bootstrap method. *J Am Stat Assoc* 1997; 92:548–560.

32. DeLong ER, DeLong DM, Clarke-Pearson DL. Comparing the areas under two or more correlated receiver operating characteristic curves: a nonparametric approach. *Biometrics* 1988; 44:837–845.

33. Landis JR, Koch GG. The measurement of observer agreement for categorical data. *Biometrics* 1977; 33:159–174.

34. Dones VC III, Grimmer K, Thoirs K, Suarez CG, Luker J. The diagnostic validity of musculoskeletal ultrasound in lateral epicondylalgia: a systematic review. *BMC Med Imaging* 2014; 14:10.